Supplement of Atmos. Meas. Tech., 13, 661–684, 2020
https://doi.org/10.5194/amt-13-661-2020-supplement

Atmospheric Measurement Techniques
Open Access
EGU

Supplement of

Comparison of aircraft measurements during GoAmazon2014/5 and ACRIDICON-CHUVA

Fan Mei et al.

Correspondence to: Fan Mei (fan.mei@pnnl.gov)

Supplemental material:

1. Additional observations

Both aircraft cannot appear at the same location at the same time due to safety concerns. Thus, the approval of a formation (inter-comparison) flight was acquired six months before the campaign through DOE Pacific Northwest Site Office (PNSO) and the Office of Aviation Management (OAM). Essential risk mitigation was also discussed and approved by the Pacific Northwest National Laboratory Aviation Risk Management Committee (PNNL ARMC). During the IOP, both aircraft crew and scientists teams set up a meeting to discuss the potential flight plan. After the flight plan was formed, both pilots briefed the plan to the Brazilian Air Force (BAF) and Airport Traffic Control (ATC). The clear-sky flight would be under Visual Flight Rules (VFR), which means good weather and no cloud, and pilots communicate with each other using an air-to-air frequency. For coordinated flights in cloudy conditions, the G1 and the HALO were both on Instrument Flight Rules (IFR) flight plan.

The coordinated flight on October 1, 2014, was initially designed to be a coordinated flight under a cloudy condition, which means the G1 and the HALO flew the same flight leg with at least 300 m altitude offset and at least 5 minutes apart. However, the coordinated two flight legs (~900 m and ~1200 m) are all below the cloud. Thus, the comparison focus on the correlation between two aircraft measurements, not vertical profiling.

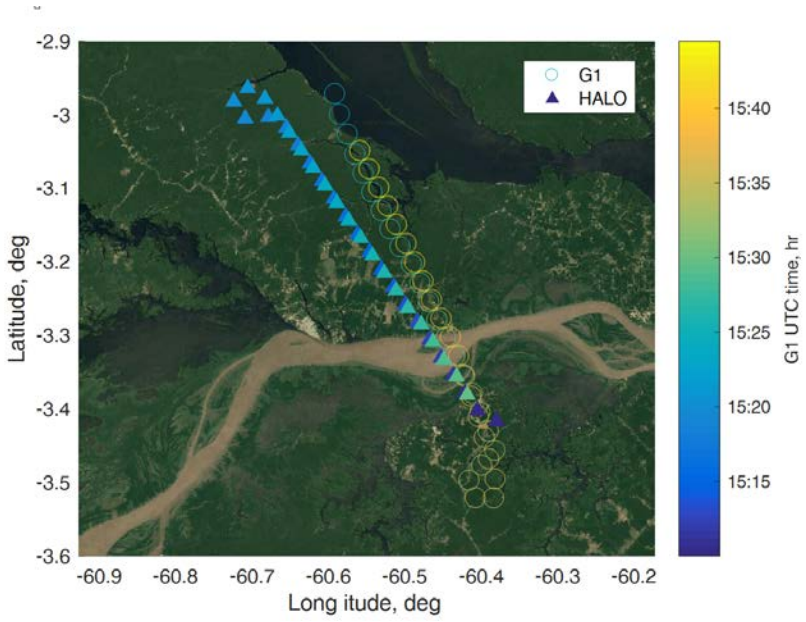

Figure S1. Time colored flight track of the G1 (circle) and the HALO (triangle) on October 1, 2014, during a cloudless coordinated flight (This figure was created using Mapping Toolbox™ © COPYRIGHT 1997–2019 by The MathWorks, Inc).

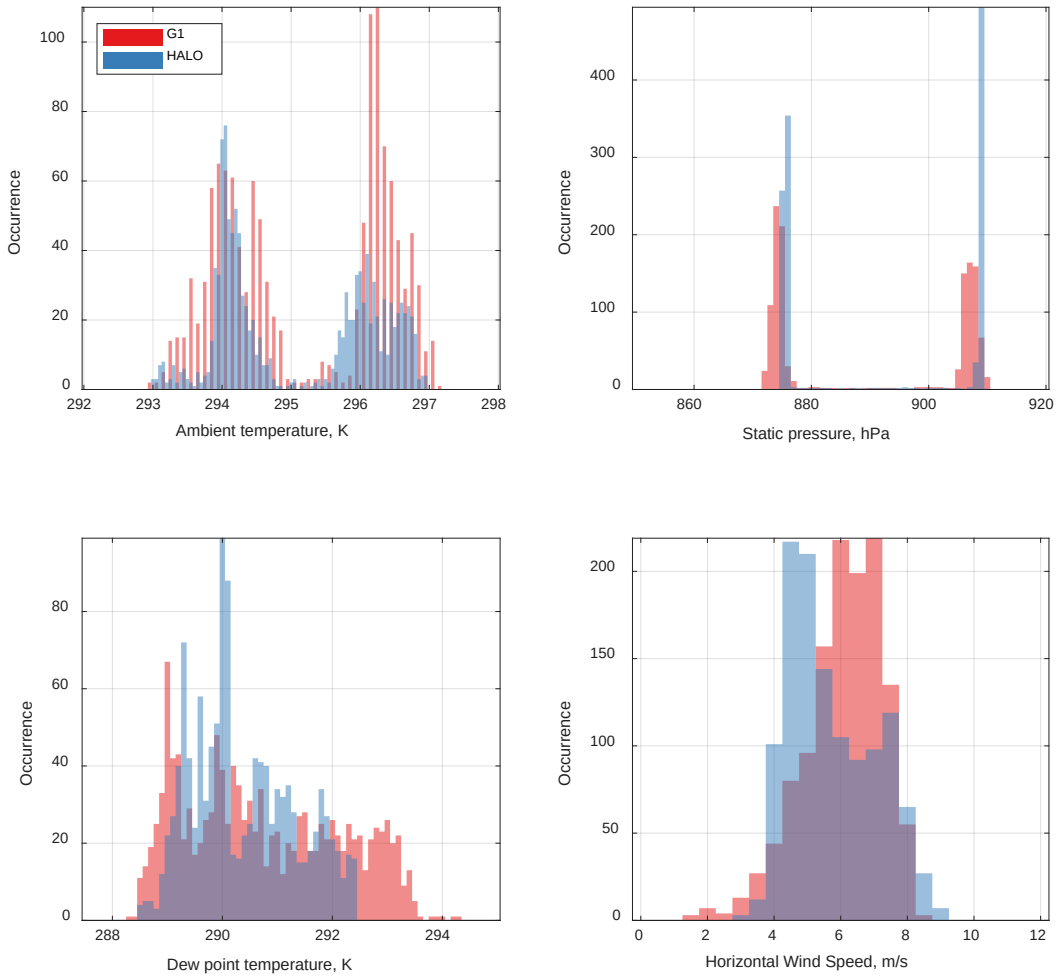

Figure S2, Atmospheric parameters observed by the G1 and the HALO on October 1, 2014.

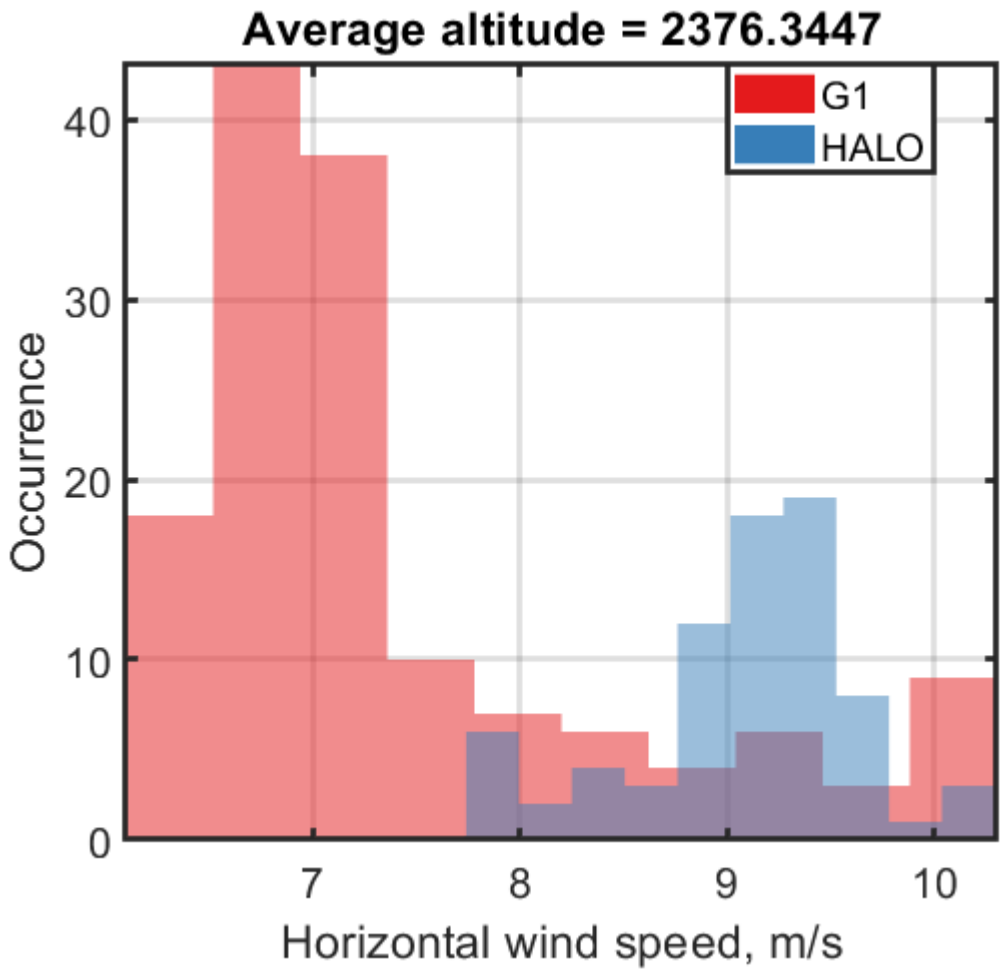

Figure S3. Horizontal wind speed between 2000-3000 m altitude on September 21, 2014.

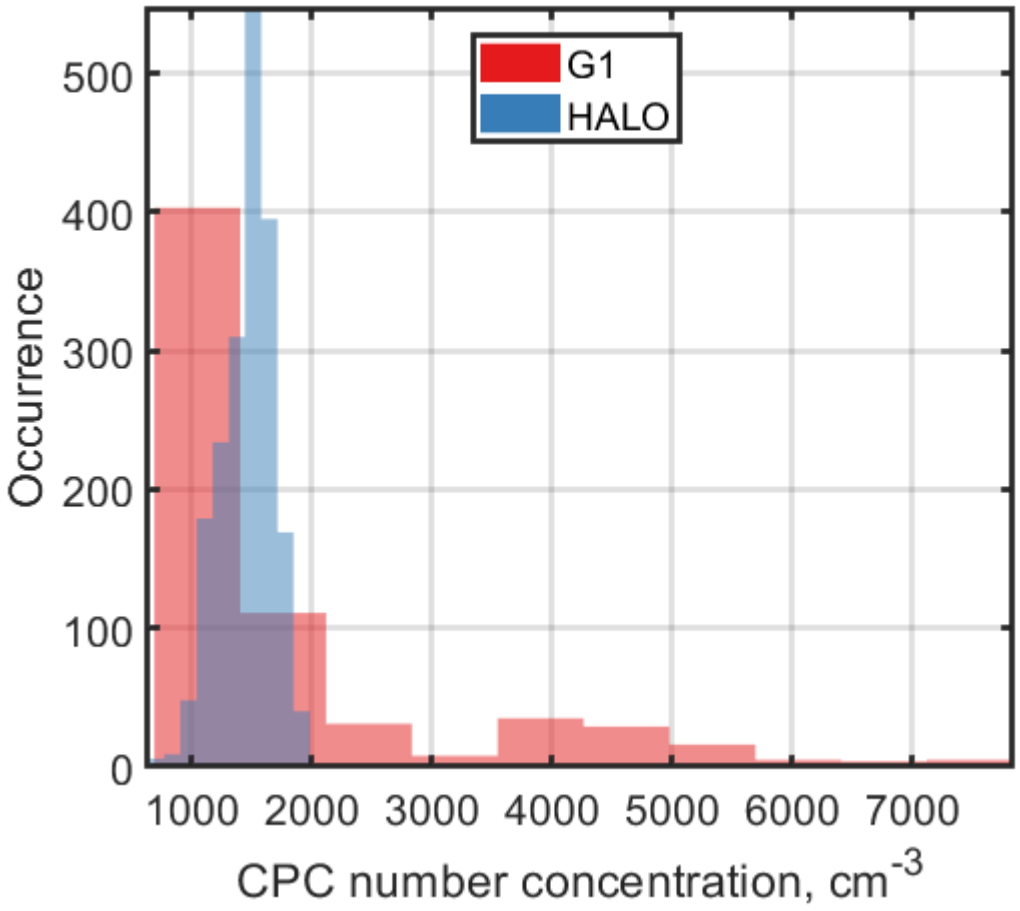
G1
HALO
Occurrence
0
100
200
300
400
500
1000
2000
3000
4000
5000
6000
7000
CPC number concentration, cm-3

(a)

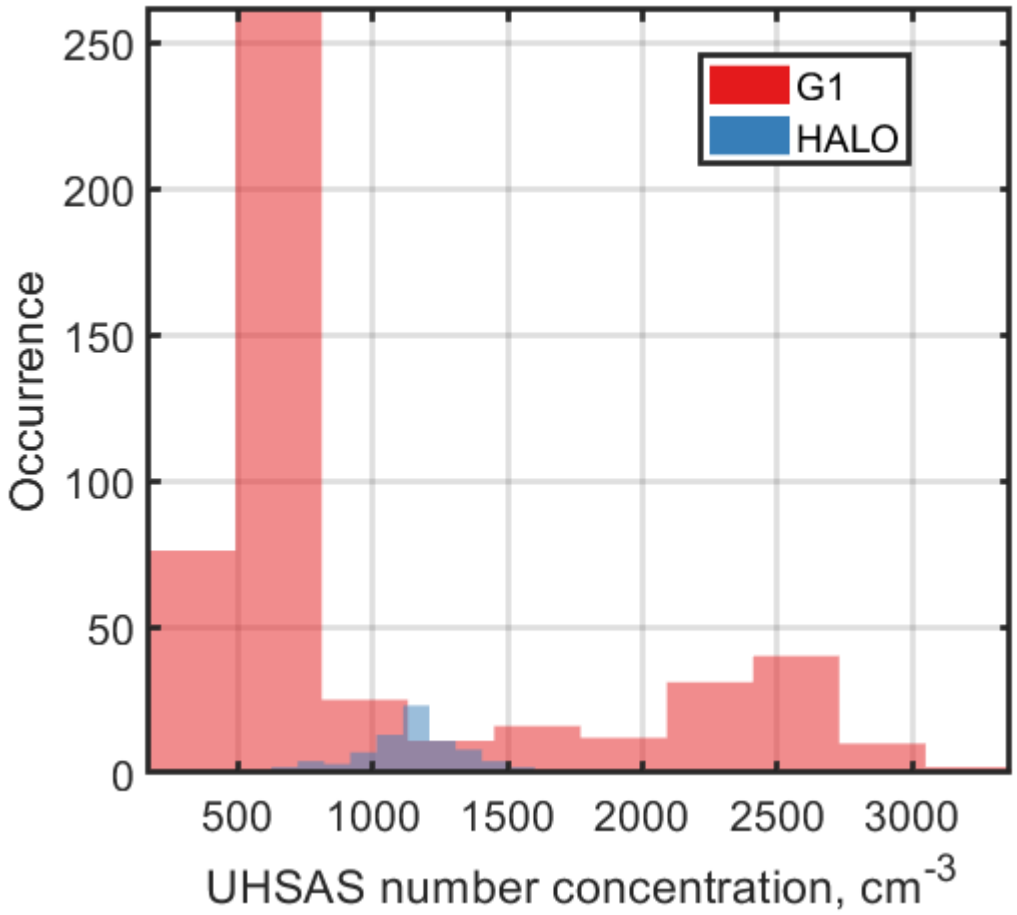

(b)

Figure S4. The total aerosol particles number concentration between 2000-3000 m altitude on September 21, 2014: (a) CPC measurement; (b) UHSAS measurement.

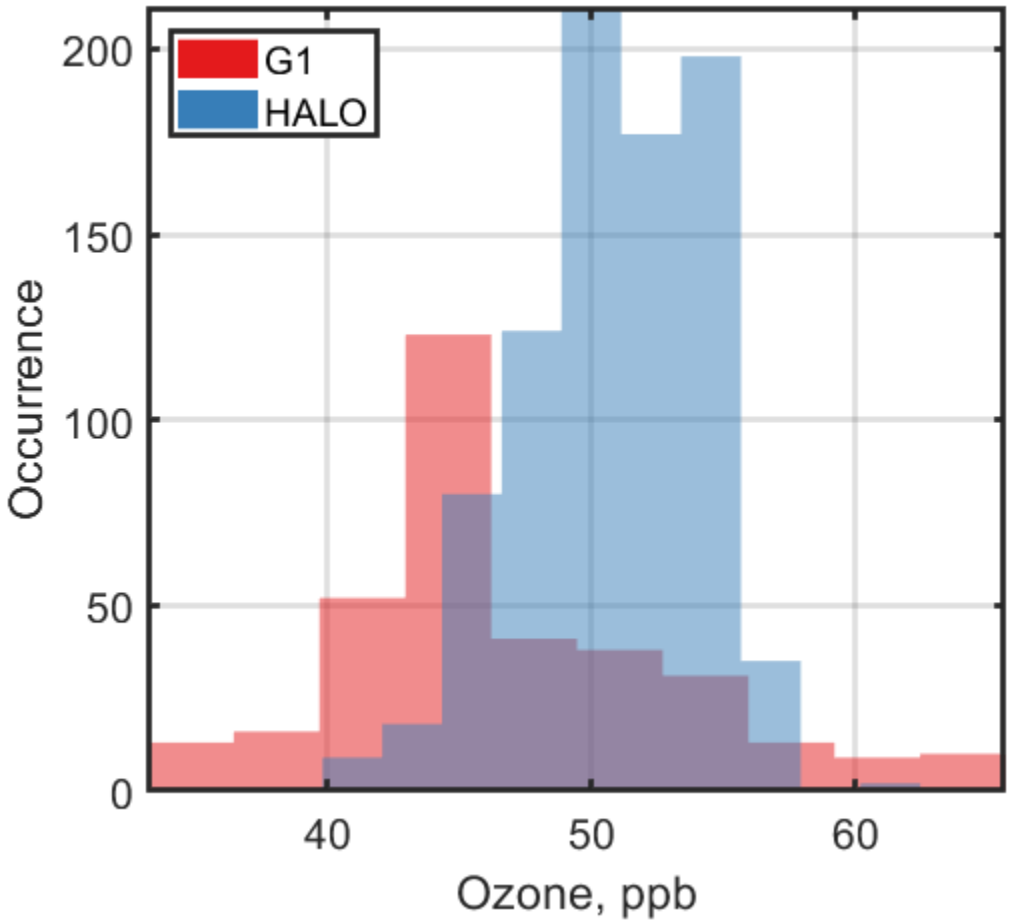

(a)

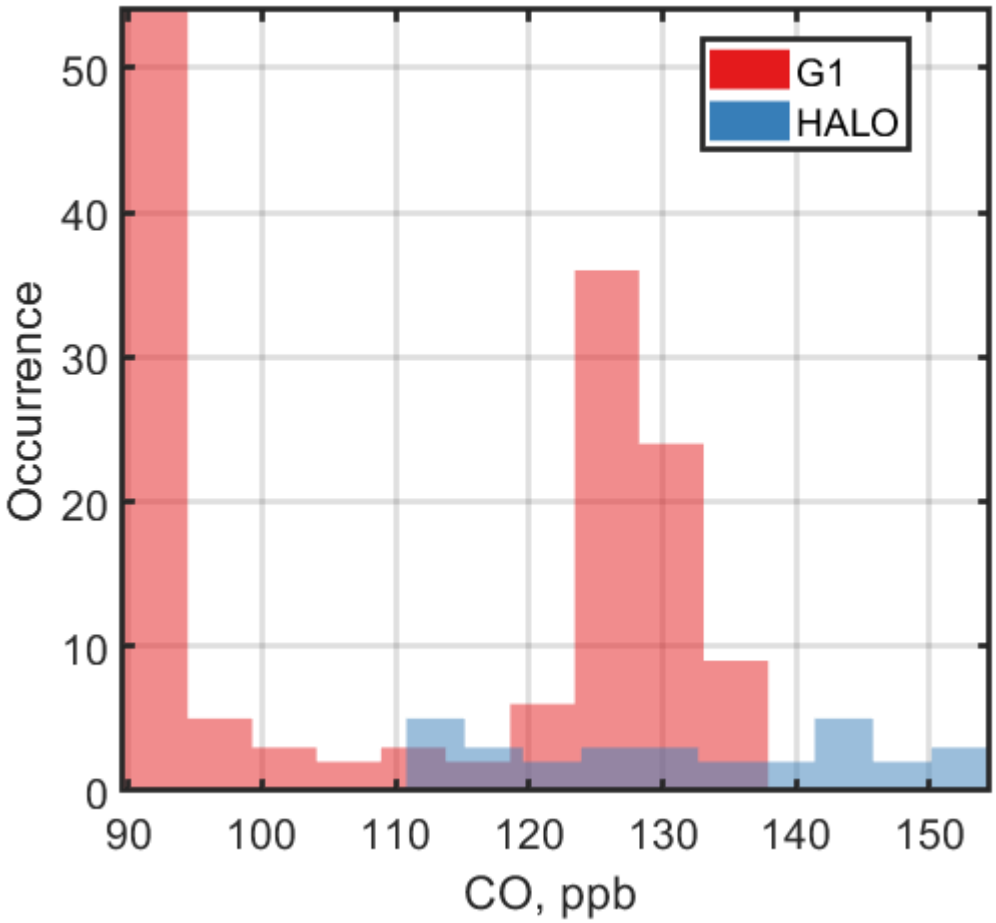

(b)

Figure S5. The trace gas concentration between 2000-3000 m altitude on September 21, 2014: (a) Ozone measurement; (b) CO measurement.

2. Additional information for AMS

Most of the details for the AMS measurements have been included in the separate AMS papers (Schulz et al., 2018; Shilling et al., 2018). Brief summaries are provided below.

The G1 AMS was operated with a constant pressure inlet (CPI), which was set to a constant pressure during the campaign. The G1 AMS was calibrated once a week during the deployment. One additional calibration was performed after the flight day, and all the calibrations were in agreement with each other. Based on five calibrations, the averaged parameters such as the

airbeam signal (AB), the ionization efficiency (IE), and the relative ionization efficiency (RIE) were applied to all of the data. A real-time correction was made to account for the variations in the AB changes to improve the instrument sensitivity. Typically, this correction is small (<20%) in absolute magnitude. The particle collection efficiency (CE) was determined by comparing AMS data to UHSAS and FIMS data. We also confirmed the CE=0.5 by comparing mass loadings observed at the T3 site to the G1 data.

The HALO AMS was calibrated before, during (twice), and after the campaign for (relative) ionization efficiencies of nitrate, ammonium, and sulfate (Schulz et al., 2018). For organics, the default relative ionization efficiency of 1.4 was assumed. The inlet flow was kept constant by the CPI and was measured before and during the campaign. Collection efficiency of 0.5 was applied, as recommended by Middlebrook et al. (2012) for low nitrate conditions. Further details on the operation of the C-ToF-AMS are given in Schulz et al. (2018).

Figure S6(a) shows vertical profiles of the total mass concentrations measured by the two AMS instruments on September 21. Above 2500 m altitude, the agreement between the two instruments is excellent (mean difference less than 5%). Between 2000 and 2500 m, the agreement is within the uncertainty range. Below 2000 m altitude, however, the aerosol particle mass concentrations measured by the AMS operated on HALO are lower than the concentrations measured by the AMS on the G1. To compare AMS data to UHSAS data, the aerosol mass concentrations of the G1 AMS were converted to the aerosol volume concentration assuming an organic compound density of 1.5 g cm^{-3} (Pöschl et al., 2010). The converted aerosol volume concentration agreed well with the volume concentration calculated based on UHSAS data, especially below 2500 m, as shown in Figure S6(b). The agreement at lower altitudes suggests that the lower concentration measured by the HALO AMS is due to the transmission efficiency issue in the constant pressure inlet used by the HALO AMS. This inlet was a prototype, designed and built at MPIC Mainz, and works by changing the size of the critical orifice that regulates the flow into the aerodynamic lens. The design and transmission characteristics will be described in an upcoming publication (Molleker, S., in prep.). The AMS aboard the G1 used a constant pressure inlet based on the design in Bahreini et al., 2008. Thus, we conclude that data above 2500 m altitude measured by the AMS aboard HALO in 2014 are valid, while data below 2500 m need to be corrected using correction factors derived from laboratory characterization before further study.

After 2014, the HALO AMS inlet design was improved to address the inlet transmission issues specific to this field campaign.

The second comparison between the two AMS conducted on October 1 is shown in Figures S6 and S7. The findings are basically in agreement with those of September 21, although the underestimation of aerosol mass concentration due to the inlet in the HALO AMS appears here to be restricted to altitudes lower than 1500 m.

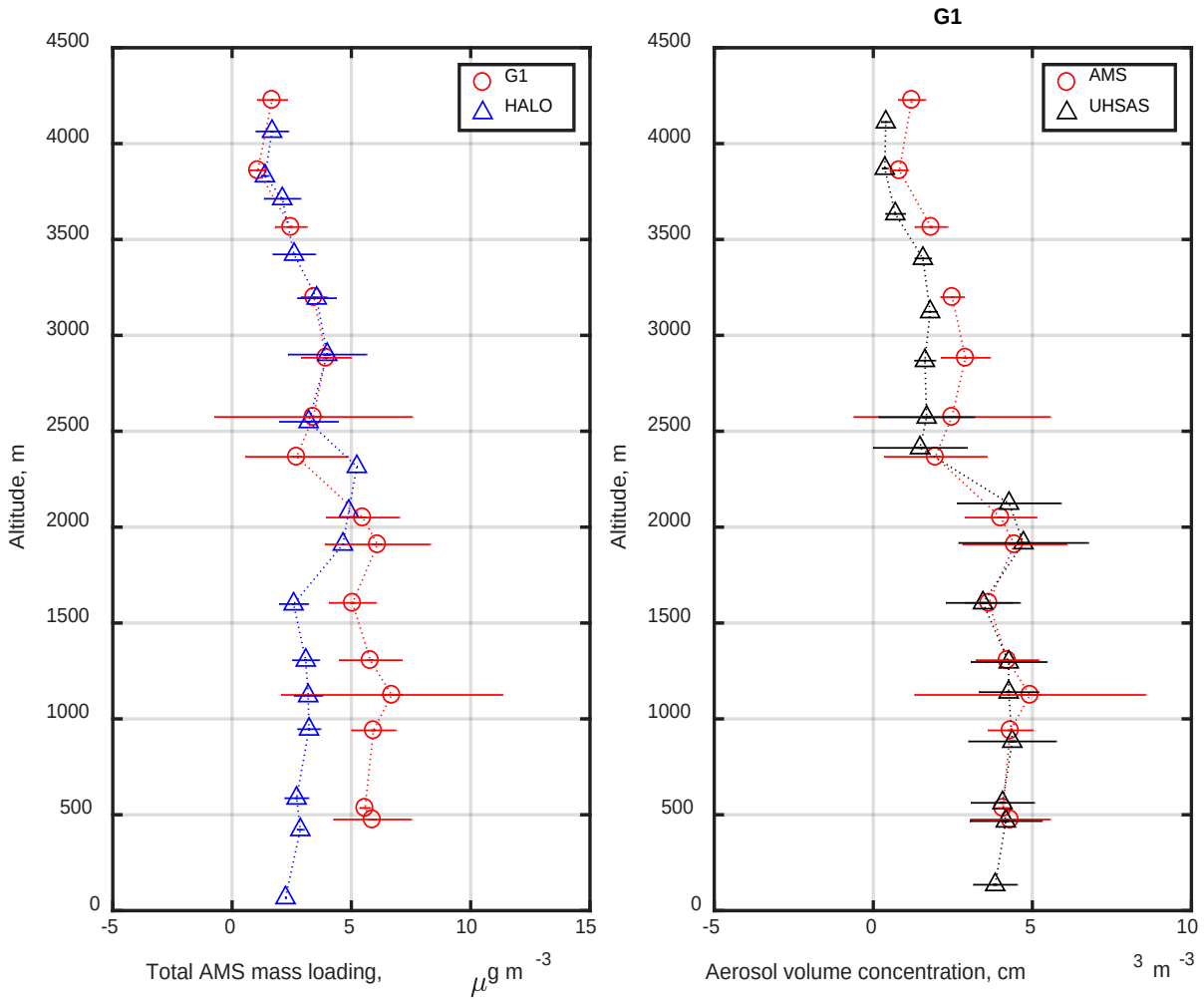

Figure S6. (a) Comparison of aerosol mass loading measured by the G1 and HALO AMS on September 21; (b) aerosol volume concentration comparison from AMS and the integrated UHSAS on the G1.

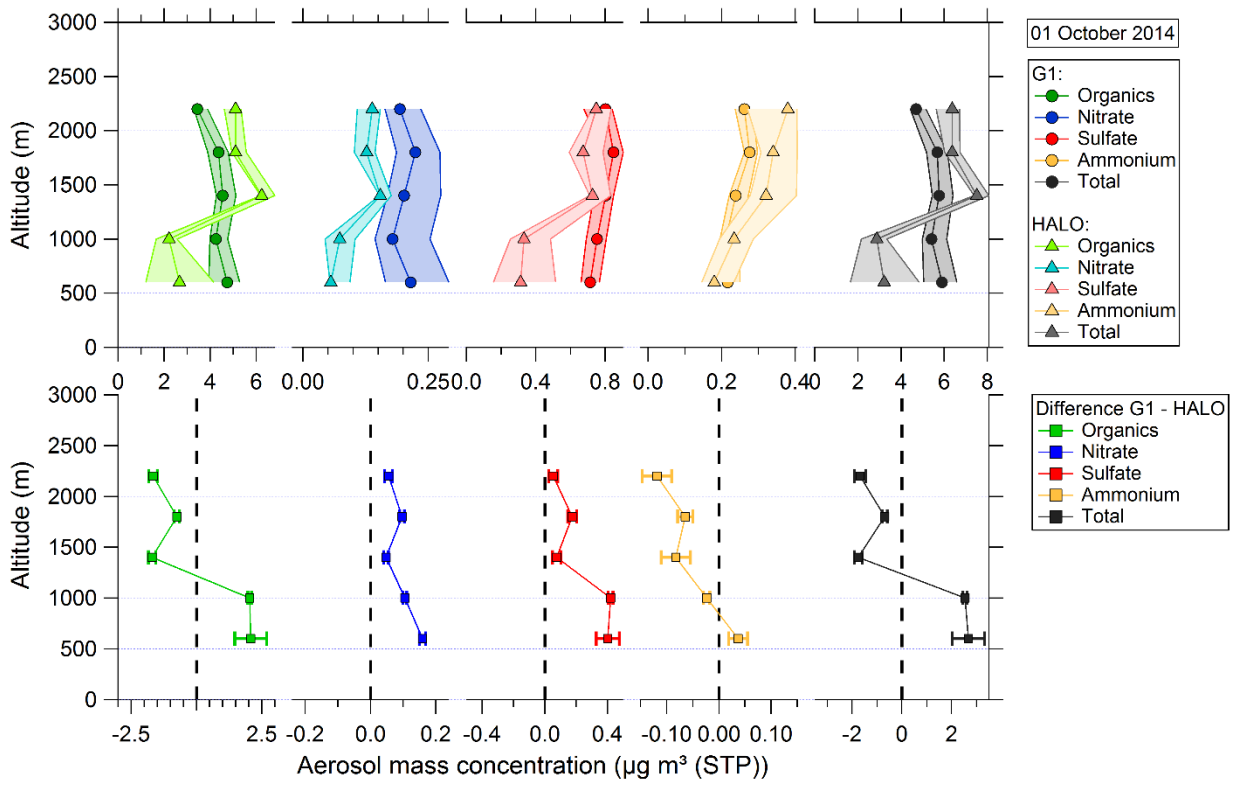

Figure S7. The vertical profiling of the aerosol mass concentration observed by the G1 and HALO during October 1.

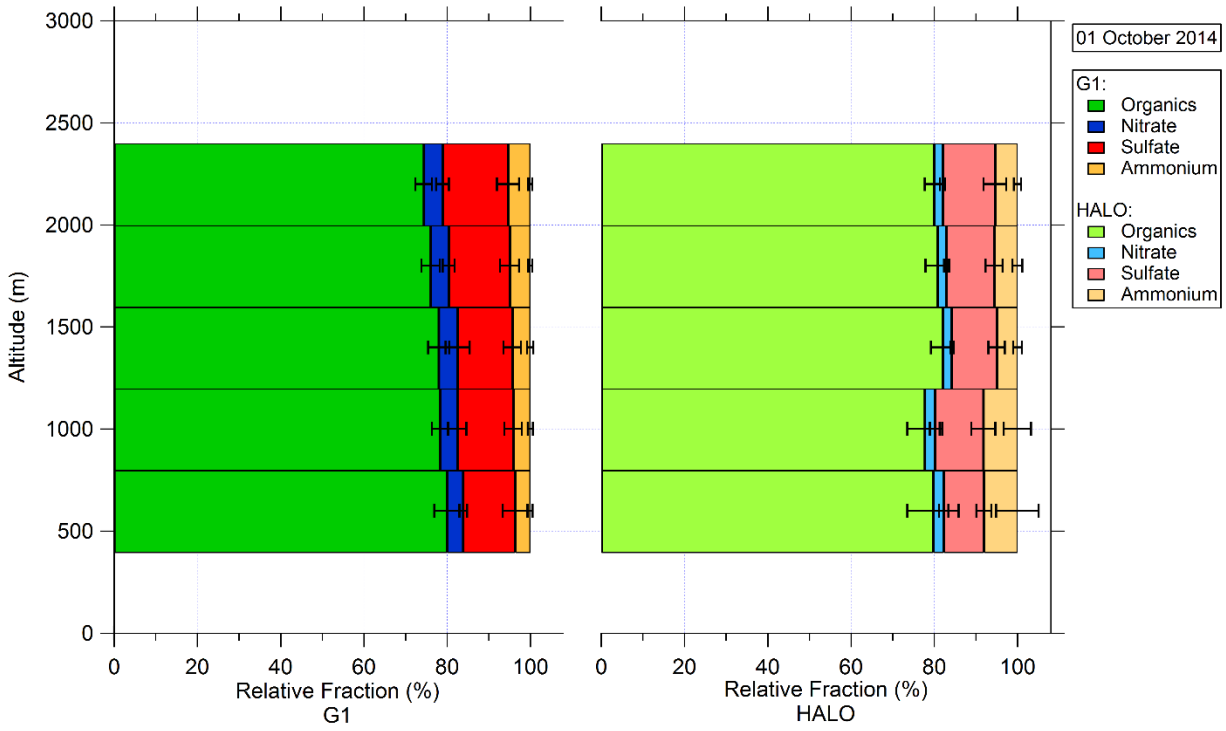

Figure S8. The vertical profiling of the relative fractions for the chemical species observed by the G1 and HALO during October 1.

3. CCN closure

To further examine the relative importance of mixing state and chemical composition, the CCN concentrations were calculated from aerosol particle size distribution, and chemical composition measured onboard the G1. The calculation was based on κ-Köhler parameterization, (Kohler, 1936; Petters and Kreidenweis, 2007, 2008, 2013) and the detail of the approach was described by Mei et al. (2013b). For the flight on September 9, 2017, the CCN number concentration calculated from the G1 UHSAS size distribution and chemical composition exhibits underestimation at a supersaturation of 0.5% (Fig, S9(a)) and when the altitude is below 1000 m (Fig S9(b)). This underestimation suggests that the UHSAS size range (90-500 nm) did not fully cover the aerosols with the critical activation diameter ($D_{p,50}$) at high supersaturation. Thus, the FIMS measurements onboard the G1 was the more appropriate size distribution for both the CCN closure study. The CCN concentration calculated using the size distribution from FIMS agrees

well with the measurement (Fig. S10). The scattering of the comparison data in Figure 15 is likely due to the chemical composition and mixing state effect on aerosol hygroscopicity.

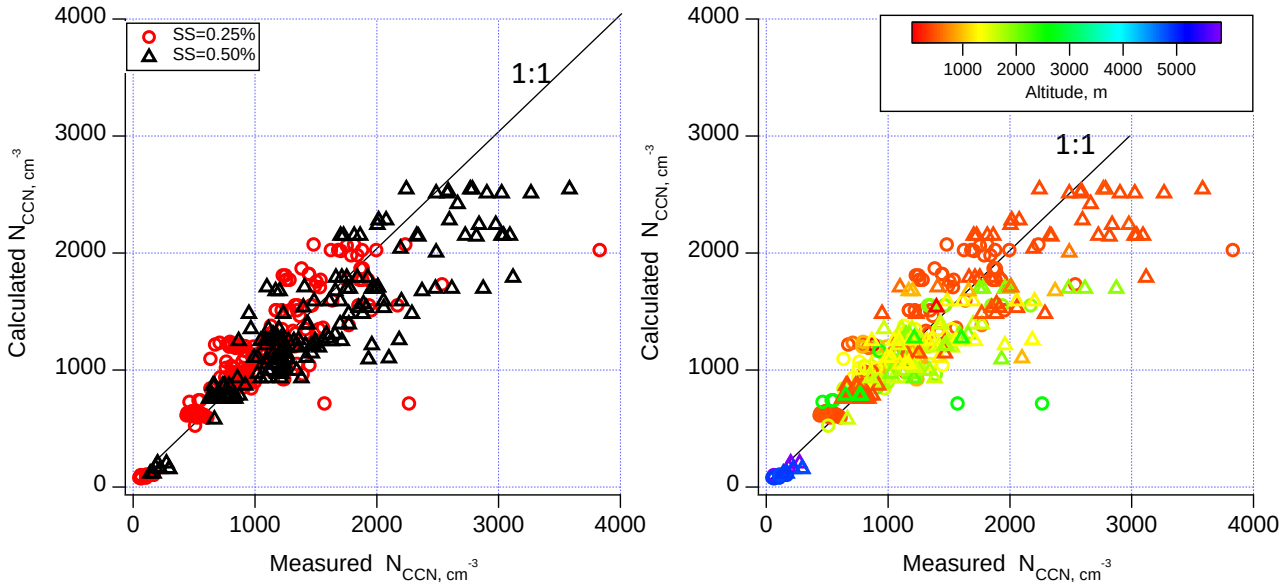

(a) (b)

Figure S9. Comparison of calculated CCN with measured CCN using the averaged 1 min measurements from the G1: (a) colored by different supersaturations. (b) colored by different altitudes. (Note that both plots used the calculated CCN number concentration from UHSAS size distribution.)

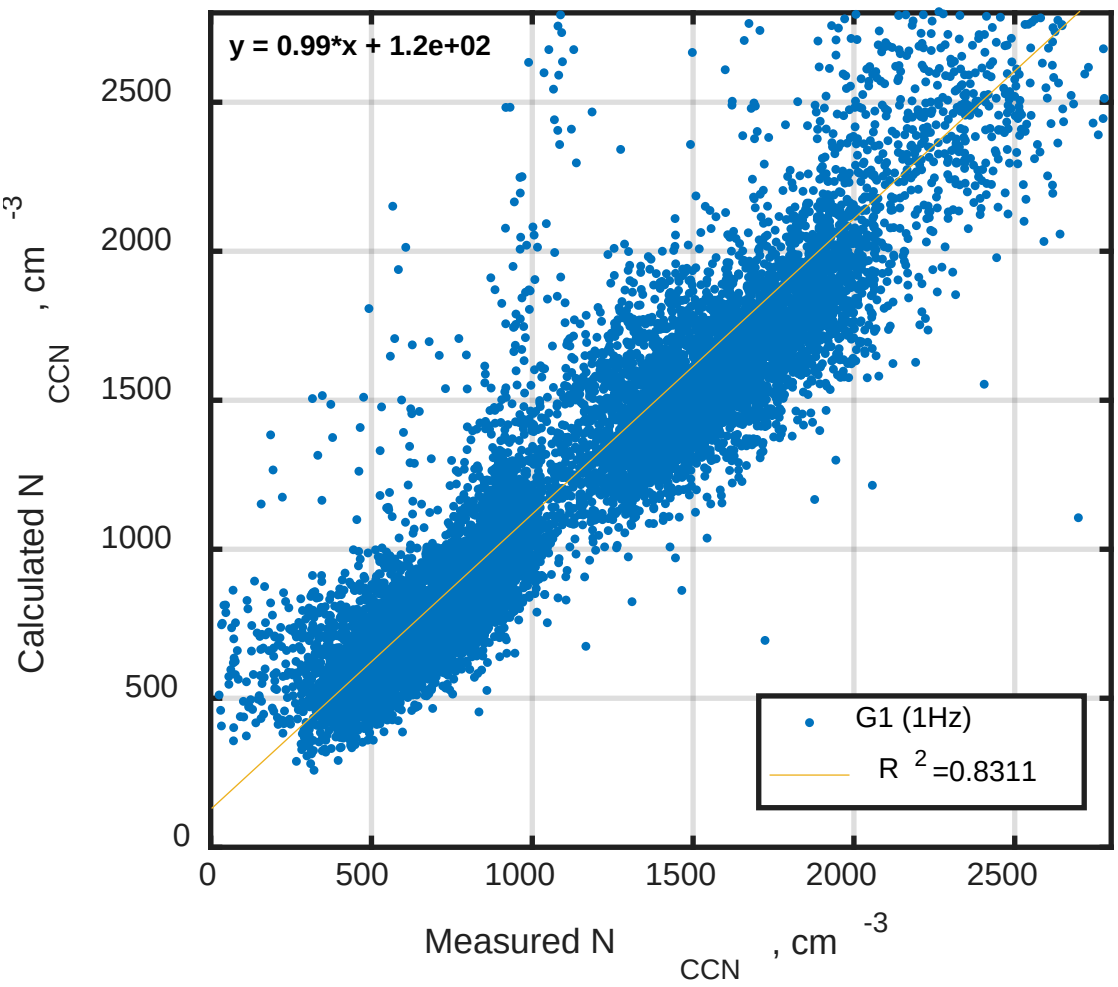

Figure S10. The scatter plot of the calculated CCN number concentration using FIMS size distribution compared with the measured CCN number concentration

4. Cloud probe observations

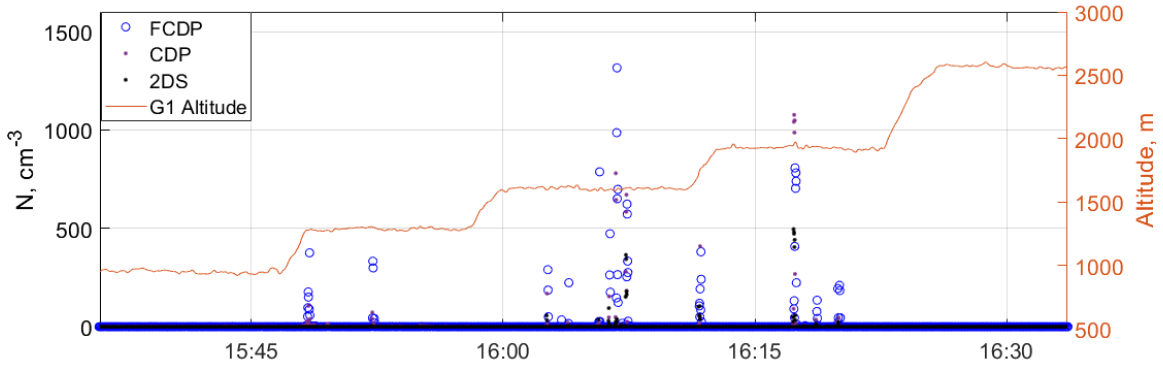

Figure S11. The cloud droplet number concentration from the G1 aircraft on September 21.

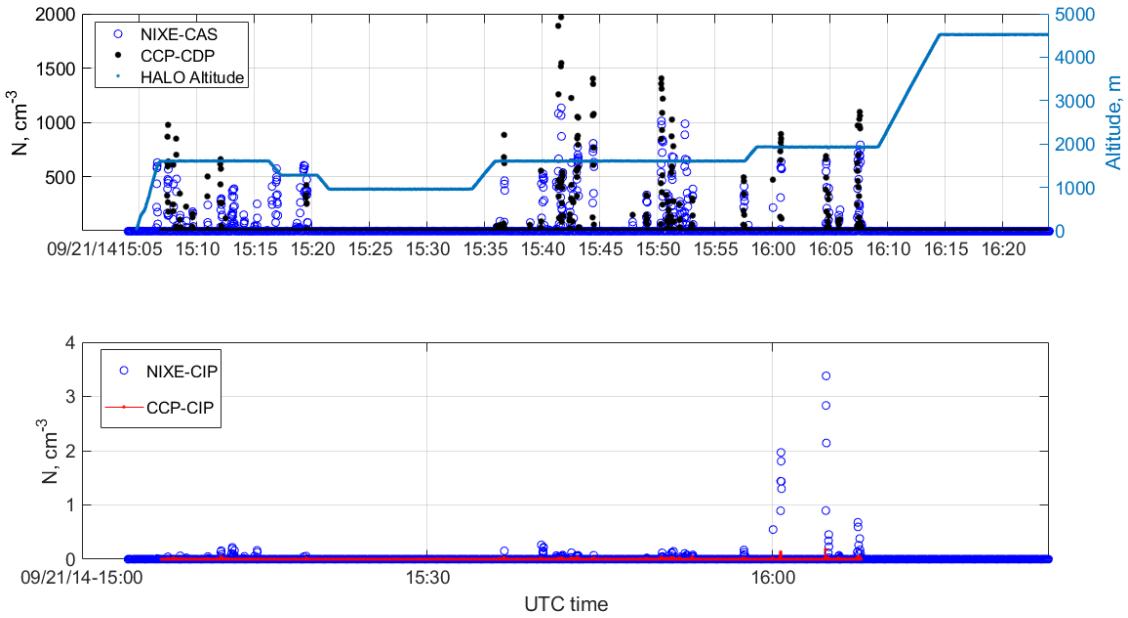

Figure S12. The cloud droplet number concentration from HALO on September 21.

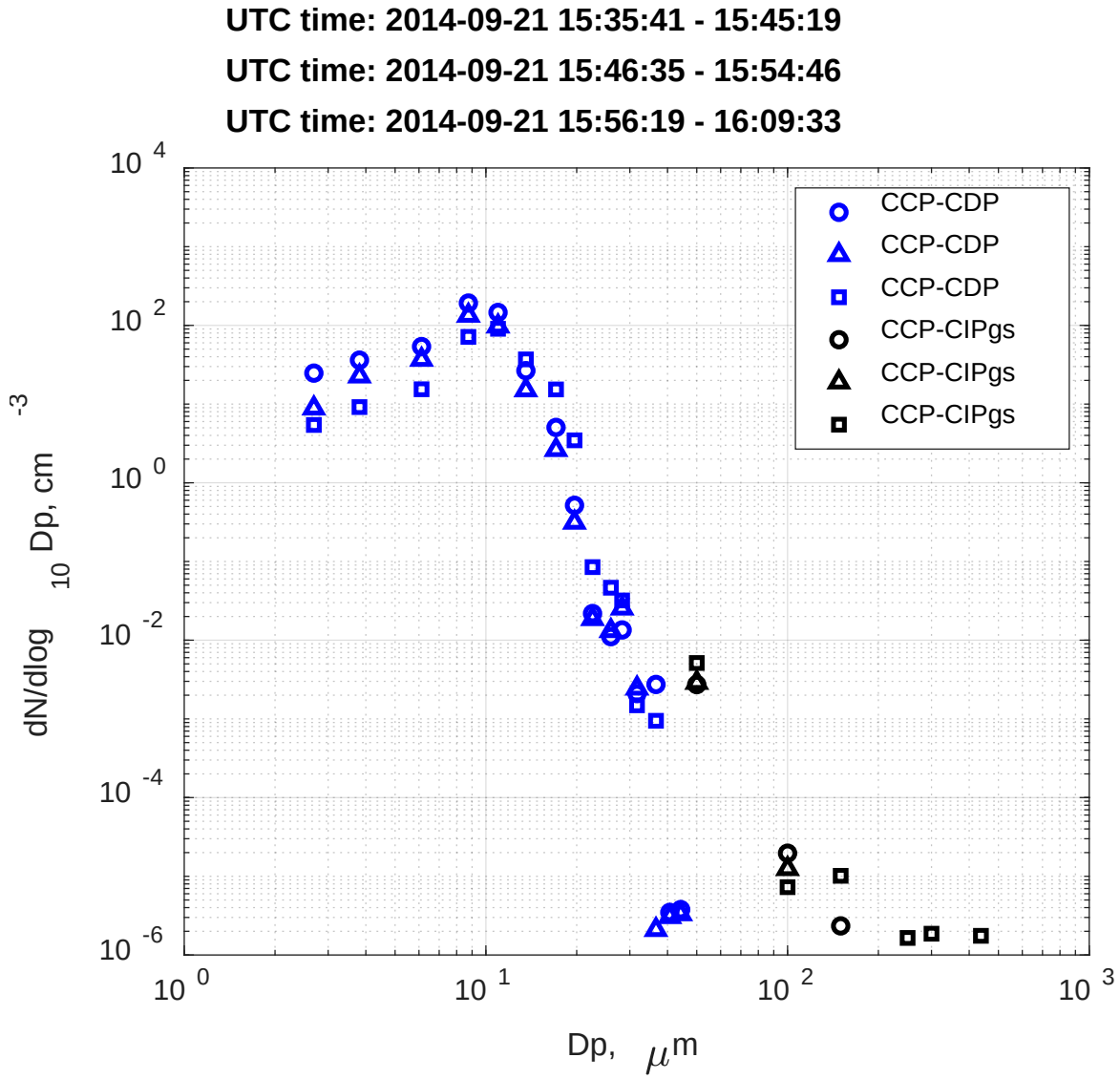
UTC time: 2014-09-21 15:35:41 - 15:45:19
UTC time: 2014-09-21 15:46:35 - 15:54:46
UTC time: 2014-09-21 15:56:19 - 16:09:33
CCP-CDP
CCP-CDP
CCP-CDP
CCP-CIPgs
CCP-CIPgs
CCP-CIPgs
dN/dlog10Dp, cm-3
Dp, μm
10 4
10 2
10 0
10 -2
10 -4
10 -6
10 0
10 1
10 2
10 3

141

142 (a)

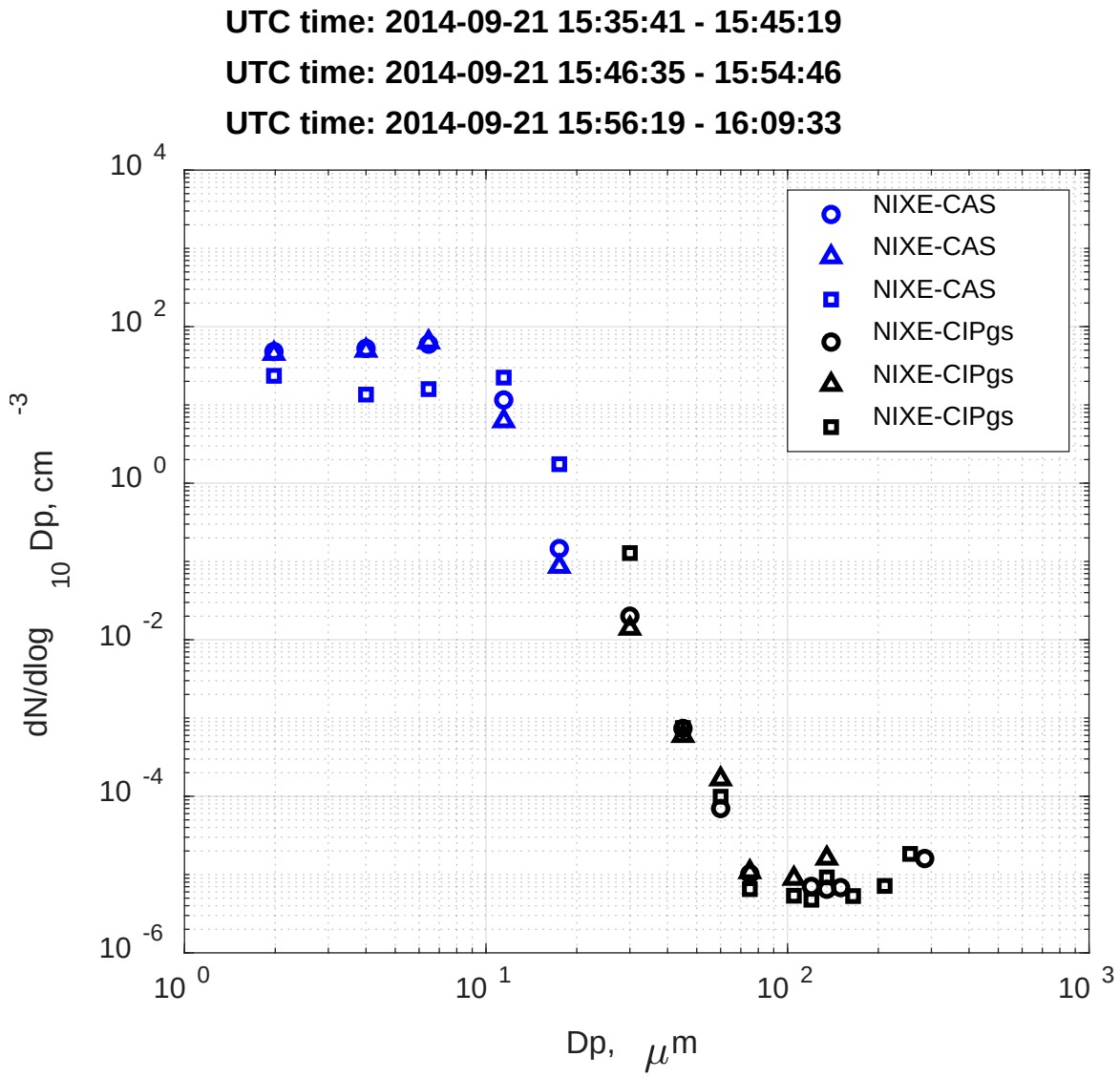
UTC time: 2014-09-21 15:35:41 - 15:45:19
UTC time: 2014-09-21 15:46:35 - 15:54:46
UTC time: 2014-09-21 15:56:19 - 16:09:33
NIXE-CAS
NIXE-CAS
NIXE-CAS
NIXE-CIPgs
NIXE-CIPgs
NIXE-CIPgs
dN/dlog10 Dp, cm-3
Dp, μm
10 4
10 2
10 0
10 -2
10 -4
10 -6
10 0
10 1
10 2
10 3

143

144 (b)

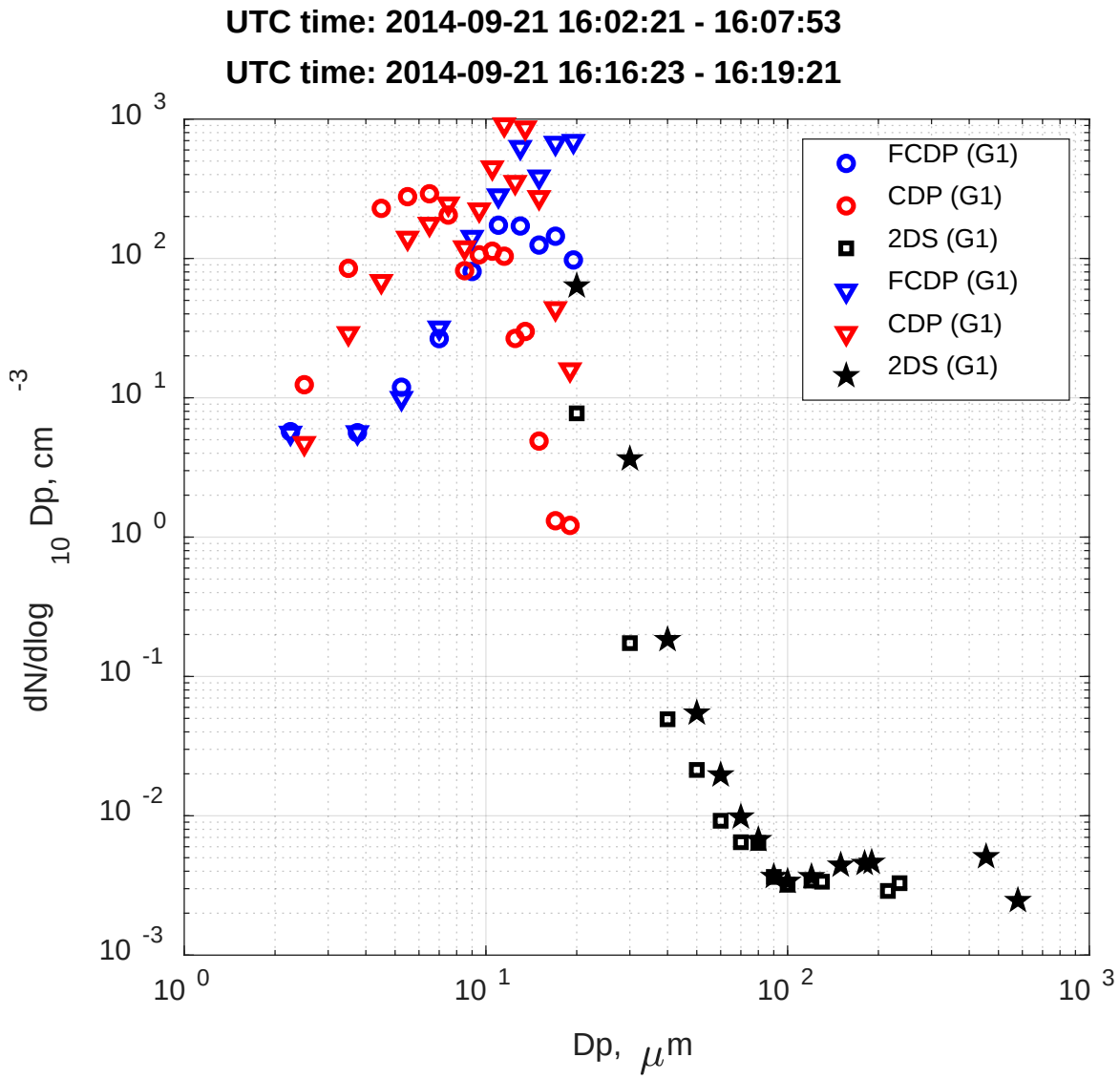

(c)

Figure S13. The averaged cloud droplet size distributions from HALO on September 21, (a) CCP probes; (b) NIXE-CAPS probes; (c) Cloud probes on board the G1.

5. Radiation measurements

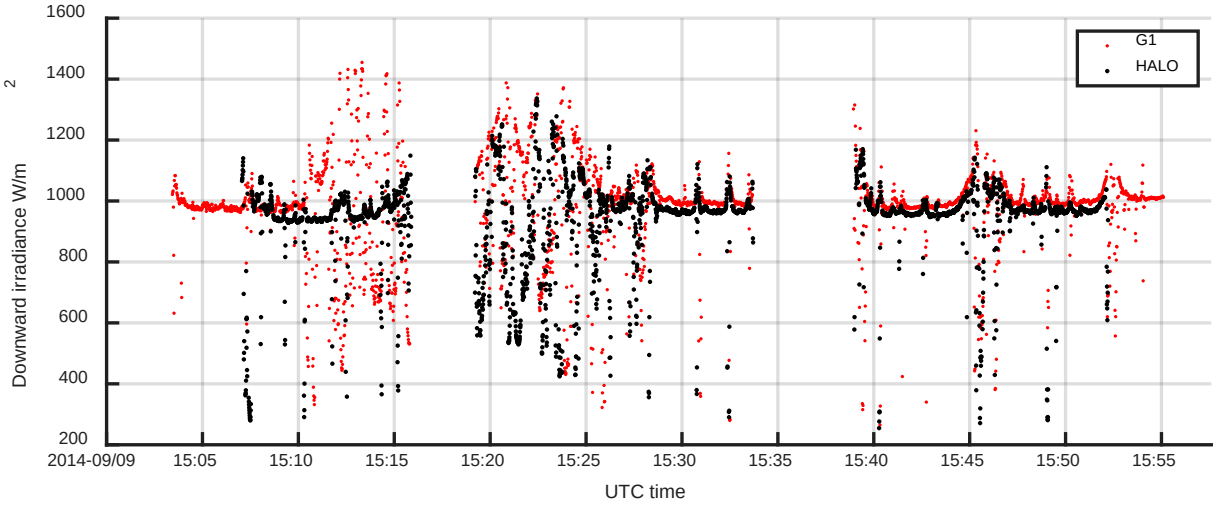

Figure S14. Time series comparison of the G1 (SPN-1) and HALO (SMART-Albedometer) radiation measurements on September 9.

Table S1. Calibration and maintenance for the instruments deployed on G1

Measurement Variables	Instruments deployed on the G1 (Martin et al., 2016; Schmid et al., 2014)	Calibration/Maintenance
Static Pressure	Rosemount (1201F1), 0-1400 hPa	Calibrated before/after each field campaign
Static air temperature	Rosemount E102AL/510BF -50 to +50 °C	Calibrated before/after each field campaign
Dewpoint temperature	Chilled mirror hygrometer 1011B -40 to +50 °C	Calibrated before/after each field campaign
3-D wind	Aircraft Integrated Meteorological Measurement System 20 (AIMMS-20)	Calibrated with Special flight pattern before each field campaign. Inter-comparison with other GPS/INS during deployment.
Particle number concentration	CPC, cut off size (D_p) =10 nm	Calibrated before/after each field campaign. Weekly calibration of sample and sheath flow rates and inter-comparisons with similar counters during deployment.
Size distribution*	UHSAS-A, 60-1000 nm.	Calibrated before/after each field campaign. Weekly check of sizing with PSL
FIMS	10 nm – 500 nm	Calibrated before/after each field campaign. Weekly calibration of sample and sheath flow rates and checks with one size PSL

Non-Refractory particle chemical composition	HR-ToF-AMS: Organics, Sulfate, Nitrate, Ammonium, Chloride, 60-1000 nm	Weekly calibrations.
CCN concentration	CCN-200, SS= 0.25, 0.5%	Calibrated before/after each field campaign. Biweekly calibration with ammonium sulfate particles.
Gas phase concentration	N2O/CO and Ozone Analyzer, CO, O_3 concentration, precision 2 ppb	Calibrated before/after each field campaign with calibration gas mixture.
CDP	2-50 μm, ΔD_p=1-2 μm	Calibrated before/after each field campaign by the vendor. Weekly check of sizing with glass beads of several sizes
FCDP	2-50 μm, ΔD_p=1-2 μm	Calibrated before/after each field campaign by the vendor. Weekly check of sizing with glass beads of several sizes
2DS	10-1000 μm	Calibrated before/after each field campaign by the vendor.
Radiation	SPN1 downward irradiance, 400-2700 nm	Calibrated before/after each field campaign

161

162 Table S2. Calibration and maintenance for the instruments deployed on HALO

Measurement Variables	Instruments deployed on HALO (Wendisch et al., 2016)	Calibration/Maintenance
Static Pressure	Instrumented nose boom tray (DLR development), 0-1400 hPa	Calibrated before/after each field campaign
Static air temperature	Total Air Temperature (TAT) inlet (Goodrich/Rosemount type 102) with an open wire resistance temperature sensor (PT100), -70 to +50 °C	Calibrated before/after each field campaign
Dewpoint temperature	Derived from the water-vapor mixing ratio, which is measured by a tunable diode laser (TDL) system (DLR development), 5-40000 ppmv	Calibrated before/after each field campaign
3-D wind	Instrumented nose boom tray (DLR development) with an air data probe (Goodrich/Rosemount) 858AJ and high-precision Inertial Reference System (IGI IMU-IIe)	Calibrated before/after each field campaign
Particle number concentration	CPC, cut off size (D_p) =10 nm	Calibrated before/after each field campaign. Weekly inter-comparisons with similar counters during deployment.
Size distribution*	UHSAS-A, 60-1000 nm.	Calibrated before/after each field campaign. Weekly check of sizing with PSL
Non-Refractory particle chemical composition	C-ToF-AMS: Organics, Sulfate, Nitrate, Ammonium, Chloride, 60-1000 nm	Calibrated before and after the campaign and twice during the campaign

CCN concentration	CCN-200, SS= 0.13-0.53%	Calibrated before/after each field campaign. Weekly calibration with ammonium sulfate particles.
Gas phase concentration	N2O/CO and Ozone Analyzer, CO, O_3 concentration, precision 2 ppb	Calibrated before/after each field campaign with calibration gas mixture.
Cloud properties*	CCP-CDP, 2.5-46 mm, ΔD_p=1-2 μm	Calibrated before/after each field campaign. Weekly check of sizing with glass beads of several sizes
	NIXE-CAS: 0.61 -52.5 μm	Calibrated before/after each field campaign. Weekly check of sizing with glass beads of several sizes
	NIXE-CIPgs, 15-960 μm	Calibrated before/after each flight with a spinning disk.
	CCP-CIPgs: 15-960 μm	Calibrated before/after each flight with a spinning disk.
Radiation	SMART Albedometer, downward spectral irradiance, 300-2200 nm	Weekly calibrations.

Table S3. List of compared measurement ranges and measurement variances caused by the spatial variation during the field campaign.

Measurement Variables	Measured Range during the Field Campaign	Measurement Variances between the Two Aircraft
Static Pressure	500 – 1010 hPa	< 1 %
Static air temperature	272 – 310 K	< 1%
Dewpoint temperature	230 -300 K	Without clouds, <1% With clouds, the measurement from the G1 can be up to 5% lower than that of HALO
3-D wind	1-15 m/s	< 40%
Particle number concentration	500 – 15,000 cm^{-3}	< 20% for CPC, <50% for UHSAS (size dependent)
Non-Refractory particle chemical composition	< 10 $\mu g \cdot m^{-3}$	< 10% above 2500 m Up to 50% below 2500 m
CCN concentration	SS=0.25%, 100 – 2000 cm^{-3}	< 10% above 2500 m Up to 50% below 2500 m
Gas phase concentration	Ozone: 15-75 ppb CO: 50-200 ppb	Ozone: < 25% CO: < 15%
Cloud droplet number concentration	3- 20 μm	<50 %
Downward irradiance	200 -1500 $W \cdot m^{-2}$	< 10%

Reference

Fan, J., Rosenfeld, D., Zhang, Y., Giangrande, S. E., Li, Z., Machado, L. A., Martin, S. T., Yang, Y., Wang, J., and Artaxo, P.: Substantial convection and precipitation enhancements by ultrafine aerosol particles, Science, 359, 411-418, 2018.

Kohler, H.: The nucleus in and the growth of hygroscopic droplets, Transactions of the Faraday Society, 32, 1152-1161, 1936.

Kotchenruther, R. A. and Hobbs, P. V.: Humidification factors of aerosols from biomass burning in Brazil, J Geophys Res-Atmos, 103, 32081-32089, 1998.

Moran-Zuloaga, D., Ditas, F., Walters, D., Saturno, J., Brito, J., Carbone, S., Chi, X. G., de Angelis, I. H., Baars, H., Godoi, R. H. M., Heese, B., Holanda, B. A., Lavric, J. V., Martin, S. T., Ming, J., Pohlker, M. L., Ruckteschler, N., Su, H., Wang, Y. Q., Wang, Q. Q., Wang, Z. B., Weber, B., Wolff, S., Artaxo, P., Poschl, U., Andreae, M. O., and Pohlker, C.: Long-term study on coarse mode aerosols in the Amazon rain forest with the frequent intrusion of Saharan dust plumes, Atmos Chem Phys, 18, 10055-10088, 2018.

Petters, M. D. and Kreidenweis, S. M.: A single parameter representation of hygroscopic growth and cloud condensation nucleus activity, Atmos Chem Phys, 7, 1961-1971, 2007.

Petters, M. D. and Kreidenweis, S. M.: A single parameter representation of hygroscopic growth and cloud condensation nucleus activity - Part 2: Including solubility, Atmos Chem Phys, 8, 6273-6279, 2008.

Petters, M. D. and Kreidenweis, S. M.: A single parameter representation of hygroscopic growth and cloud condensation nucleus activity - Part 3: Including surfactant partitioning, Atmos Chem Phys, 13, 1081-1091, 2013.

Pöschl, U., Martin, S., Sinha, B., Chen, Q., Gunthe, S., Huffman, J., Borrmann, S., Farmer, D., Garland, R., and Helas, G.: Rainforest aerosols as biogenic nuclei of clouds and precipitation in the Amazon, Science, 329, 1513-1516, 2010.

Schulz, C., Schneider, J., Amorim Holanda, B., Appel, O., Costa, A., de Sá, S. S., Dreiling, V., Fütterer, D., Jurkat-Witschas, T., Klimach, T., Krämer, M., Martin, S. T., Mertes, S., Pöhlker, M. L., Sauer, D., Voigt, C., Weinzierl, B., Ziereis, H., Zöger, M., Andreae, M. O., Artaxo, P., Machado, L. A. T., Pöschl, U., Wendisch, M., and Borrmann, S.: Aircraft-based observations of isoprene epoxydiol-derived secondary organic aerosol (IEPOX-SOA) in the tropical upper troposphere over the Amazon region, Atmos. Chem. Phys. Discuss., 2018, 1-32, 2018.

Shilling, J. E., Pekour, M. S., Fortner, E. C., Artaxo, P., Sá, S. d., Hubbe, J. M., Longo, K. M., Machado, L. A., Martin, S. T., and Springston, S. R.: Aircraft observations of the chemical composition and aging of aerosol in the Manaus urban plume during GoAmazon 2014/5, Atmos Chem Phys, 18, 10773-10797, 2018.

Wang, J., Krejci, R., Giangrande, S., Kuang, C., Barbosa, H. M., Brito, J., Carbone, S., Chi, X., Comstock, J., Ditas, F., Lavric, J., Manninen, H. E., Mei, F., Moran-Zuloaga, D., Pohlker, C., Pohlker, M. L., Saturno, J., Schmid, B., Souza, R. A., Springston, S. R., Tomlinson, J. M., Toto, T., Walter, D., Wimmer, D., Smith, J. N., Kulmala, M., Machado, L. A., Artaxo, P., Andreae, M. O., Petaja, T., and Martin, S. T.: Amazon boundary layer aerosol concentration sustained by vertical transport during rainfall, Nature, 539, 416-419, 2016.

Williamson, C., Kupc, A., Wilson, J., Gesler, D. W., Reeves, J. M., Erdesz, F., McLaughlin, R., and Brock, C. A.: Fast time response measurements of particle size distributions in the 3-60 nm size range with the nucleation mode aerosol size spectrometer, Atmos Meas Tech, 11, 3491-3509, 2018.